Glowing avalanches from the 1974 eruption of the volcano Fuego, Guatemala

DAVID K. DAVIES*
MICHAEL W. QUEARRY*
Department of Geology, University of Missouri at Columbia, Columbia, Missouri 65201
SAMUEL B. BONIS
División Geológica, Instituto Geográfico Nacional, Avenida las Americas, Guatemala City, Guatemala

ABSTRACT

Glowing avalanches from the 1974 eruption of the volcano Fuego, Guatemala, deposited between 0.005 and 0.01 km^3 of nonimbricated, nongraded, nonwelded debris on the southern flanks of the volcano. Avalanches emerged from notches in the crater rim, and traveled some 7 km from the vent at an average speed of 60 km/hr. Each glowing avalanche consisted of two parts, (1) the main mass of moving debris, or underflow, and (2) a superjacent gas and dust cloud. The postdepositional thickness of individual underflows is generally less than 2 m, but successions of glowing avalanches produced deposits as much as 15 m thick in some ravines. The underflows and their superjacent gas and dust clouds followed topographic lows. Where underflows were confined laterally by valley walls, the surface of the underflow was featureless, after deposition. Where underflows were able to spread laterally, they developed a surface morphology of channels, levees, and overbank areas. The coarsest fragments were deposited in the channels.

The underflows probably flowed in laminar fashion as high concentration dispersions, similar to normal debris flows. No unequivocal evidence of large-scale gas expansion of the underflows was noted. Gas emission is considered to have occurred during transportation, but it probably played a minor role in fluidization of the underflow. The ability of these glowing avalanches to transport particles as much as 5 m in diameter some 7 km from the crater is considered to be a reflection of the high yield strength of the underflow.

Deposits from the 1974 eruption had a mean grain size of -3.0ϕ (8 mm), were extremely poorly sorted (σ_I = 4.6) strongly fine skewed (SK_I = 0.63), and platykurtic (K_G = 0.71). All grain size distributions were bimodal with a dominant intermodal low at -1.0ϕ (2 mm). The small percentage of particles in the -1.0ϕ size interval is considered to reflect the inherent mechanical instability of particles of this size.

Turbulently flowing gas and dust clouds, as much as 1,000 m high, accompanied each avalanche, and cloud height increased with increasing distance of travel. The fine-grained dust of the superjacent gas and dust clouds was not deposited on top of the underflow. Prevailing winds blew the fine-grained component to the west-southwest.

* Present address: (Davies) Department of Geosciences, Texas Tech University, Lubbock, Texas 79409. (Quearry) Texaco, Inc., P.O. Box 60252, New Orleans, Louisiana 70160.

INTRODUCTION

The volcano Fuego in Guatemala (Figs. 1 and 2) is one of the most active volcanoes of the Americas. It is a stratovolcano composed primarily of pyroxene-andesite (Williams, 1960). Since 1524, more than 50 eruptions have been reported. Glowing avalanches have been characteristic of its many recorded eruptions, with lava production being limited to seven eruptions since 1524 (Bonis and Salazar, 1973; Pough and Mulford, 1957; Sapper, 1927; Stoiber, 1974; Williams, 1960). Ejecta from the most recent eruptions have consisted of high alumina basalts (Bonis and Salazar, 1973; Rose and others, 1973; Stoiber and Rose, 1970).

The October 1974 eruption of Fuego was similar in character to previous recorded eruptions, in that no lava flows were produced. At least 0.6 $km^3$of tephra was ejected as glowing avalanches and airfall ash, with glowing avalanches comprising between 0.005 and 0.01 km^3 of total ejecta. Two qualitative electron microprobe analyses of compressed powder pellets, one of glowing avalanche deposit and the other of airfall ash, indicate that the 1974 eruption produced high-alumina basalt with approximately 48% SiO_2 and 18% Al_2O_3 (C. K. Barsky, 1976, personal commun.).

The 1974 eruptive cycle commenced on October 10, and involved four main episodes of tephra ejection on October 14, 17, 19–20, and 23. Each volcanian eruption included the development of ash columns which reached heights of greater than 7 km above the vent, accompanied by numerous glowing avalanches (Fig. 3). Glowing avalanches emerged from notches in the crater rim, one located on the southwest, the other on the southeast side (Fig. 4). Ravines leading south from the crater were filled to depths of up to 15 m with poorly sorted, nonwelded, nonimbricated, nonstratified debris from a succession of glowing avalanches (Fig. 5). The progress of individual avalanches was recorded by time-lapse photography (Figs. 6 and 7).

Inasmuch as glowing avalanches are the products of volcanic eruptions, they are usually ignored by sedimentologists, who consider them to be more the province of the volcanologist. However, such avalanches also are ignored by volcanologists or described in qualitative terms. Several such descriptions have been published since the original vivid accounts of the 1902 eruptions of Soufrière Volcano (Anderson and Flett, 1903; Bemmelen, 1949; Hay, 1959; Lacroix, 1903; Moore and Nelson, 1969; Smith, 1960; Rose, 1973). The few quantitative descriptions of glowing avalanches have concentrated mainly on grain size analyses (Fenner, 1923; Moore, 1934; Taneda, 1954, 1957; Taneda and others, 1957).

Geological Society of America Bulletin, v. 89, p. 369–384, 26 figs., 5 tables, March 1978, Doc. no. 80305.

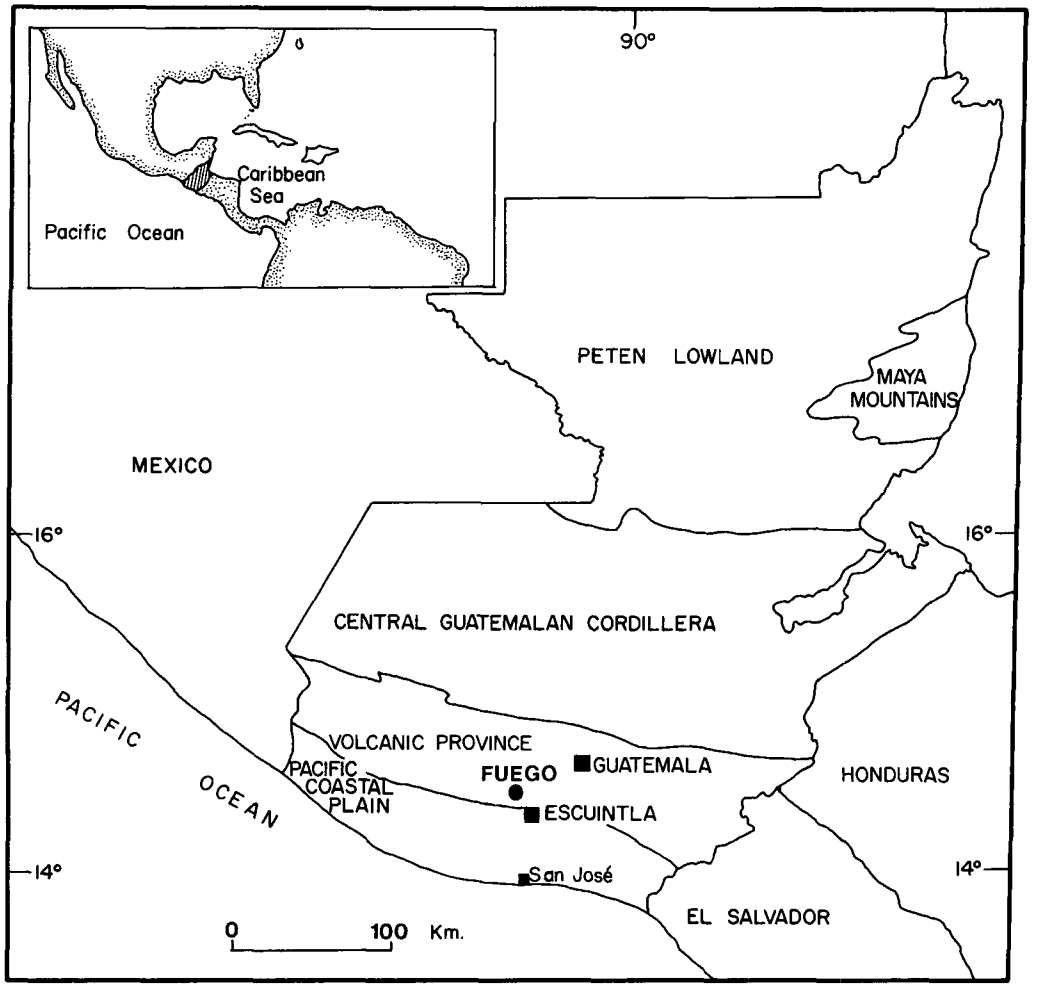

Figure 1. Location of the volcano Fuego with respect to the geologic provinces and principal cities of Guatemala.

Figure 2. Fuego (left) and its twin stratovolcano Acatenango (right).

Figure 3. Ash pillar and glowing avalanche gas clouds, 1974 eruption of Fuego. (Photo taken looking northeast; vertical relief from trees to crater is 2,700 m.)

Probably the most exhaustive quantitative studies to date are those of Murai (1961) and Sparks (1976), which centered on deposits of ancient glowing avalanches and other pyroclastic flows.

The present study deals with glowing avalanche deposits that were observed during transportation and deposition and sampled before they were modified by rainfall. It focuses attention on the glowing avalanche deposits of one ravine, Quebrada el Pajal (Figs. 5 and 8), the most accessible and least dangerous of all the ravines on the southern flanks of Fuego. It is situated at an angle to the main topographic lows, which swing to west and north of Quebrada el Pajal. Thus, glowing avalanche deposits in this ravine are thinner than in ravines on either side.

SAMPLING AND ANALYTICAL TECHNIQUES

General Statement

In Guatemala, torrential seasonal rains erode glowing avalanche deposits, often producing lahars which, in turn, grade downslope

into stream deposits. This study of the sedimentology of a glowing avalanche deposit is the forerunner of continuing sedimentologic investigations based on joint research with the Instituto Geográfico Nacional de Guatemala, dealing with the glowing avalanche–lahar-stream depositional continuum. Collection of the sort of textural, compositional, and sedimentary data as are presented herein will hopefully lead to the development of models to delineate each process in this depositional continuum.

The wide range of grain sizes represented in the glowing avalanche deposit (4μ to 5 m) posed a major problem with respect to all facets of sampling and analysis. Particles with a long axis (A) greater than 30 cm were ignored in the quantitative analysis because of their unmanageable size. However, they were included in qualitative aspects of the study. Particles with an A axis less than 30 cm were divided into two categories: (1) grains, consisting of particles with A-axes less than 30 but greater than 2.5 cm; and (2) matrix, consisting of particles with A-axes less than or equal to 2.5 cm. Both grains and matrix were analyzed for size and lithology. Shape analyses were restricted to the grains.

A tape and Brunton compass topographic map of glowing avalanche deposits in El Pajal was constructed (Fig. 9) to provide a base from which the sampling plan was established. Time-lapse photography and actual observations aided interpretations of avalanche flow.

Sampling

Samples were collected from 50 sites located along seven sample traverses oriented perpendicular to the flow direction of the avalanche deposit (Fig. 9). Eight sample sites were pits dug 1 m deep into the deposit; the remainder were surface sites. The number of sample sites per traverse depended on the range of lateral variation in morphology and grain size of the deposit. Along sample traverses which transected areas of distinctly different grain size and surface morphology, two surface sample sites were located in each distinct area. Thus, along sample line 180 (Fig. 9), 12 surface sites were necessary because of a high degree of lateral variation. Lateral variability was low along lines 20, 880, 1230, and 1390, and the number of surface sample sites along these lines ranged from 4 to 6. Pits were dug along sampling lines 180, 460, and 880 where it was considered that information return would be maximized.

A standard sampling procedure was followed at each sample site. Twenty-six grains were selected randomly, using a sampling grid (Fig. 10). This grid consisted of a 1-m square framework with twine strung between nailheads spaced 5 cm apart on opposite sides of the frame. A unique coordinate for each twine intersection was established by numbering each strand of twine from 1 to 19. Random number tables were used to select the 26 twine intersection coordinates at which one grain was sampled for lithology and shape analysis. Matrix samples, collected only from the pits, were taken by inserting a cylindrical can, 10 cm by 10 cm, into the wall of each 1-m-deep pit at two randomly selected coordinates.

Size Analyses

General Statement. The wide range of particle size in glowing avalanche deposits presents a particularly difficult problem with respect to size analyses. In the field of sedimentology, most techniques of size analyses yield data that are expressed in terms of weight percent. Sieve analyses or grain-settling techniques are routinely used to yield weight percent data in sand- and silt-sized sediments. Such techniques cannot be used in sediments which contain a significant proportion of material coarser than sand size.

Figure 4. Notch on southeast side of the crater of Fuego (notch is ~ 60 m deep).

However, it is vital to generate reproducible and compatible data for both coarse and fine size fractions. We have chosen to report all of our size data in terms of weight percent, and this involves the transformation of size data generated for grains.

Grains. The length of the intermediate (B) axis of each grain was taken as the size of that grain, and each grain was assigned to its respective phi size class at ½ϕ intervals. Weight computations for grains (particles 2.5 to 30.0 cm) utilized measurements of long (A), intermediate (B), and short (C) axes. In this technique, each grain was considered to be a triaxial ellipsoid, and the volume of each grain was computed and then multiplied by its density to obtain the weight of the grain. (Density measurements were undertaken in the laboratory using representative samples of vesicular basalt. Densities ranged from 2.36 g/cc to 2.44 g/cc, with a mean of 2.40 g/cc).

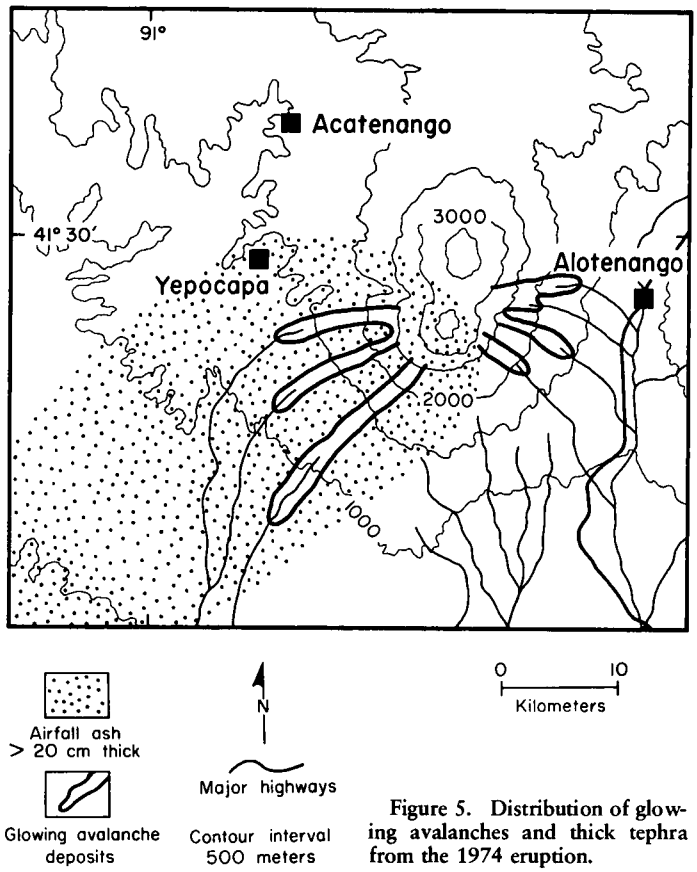

Figure 5. Distribution of glowing avalanches and thick tephra from the 1974 eruption.

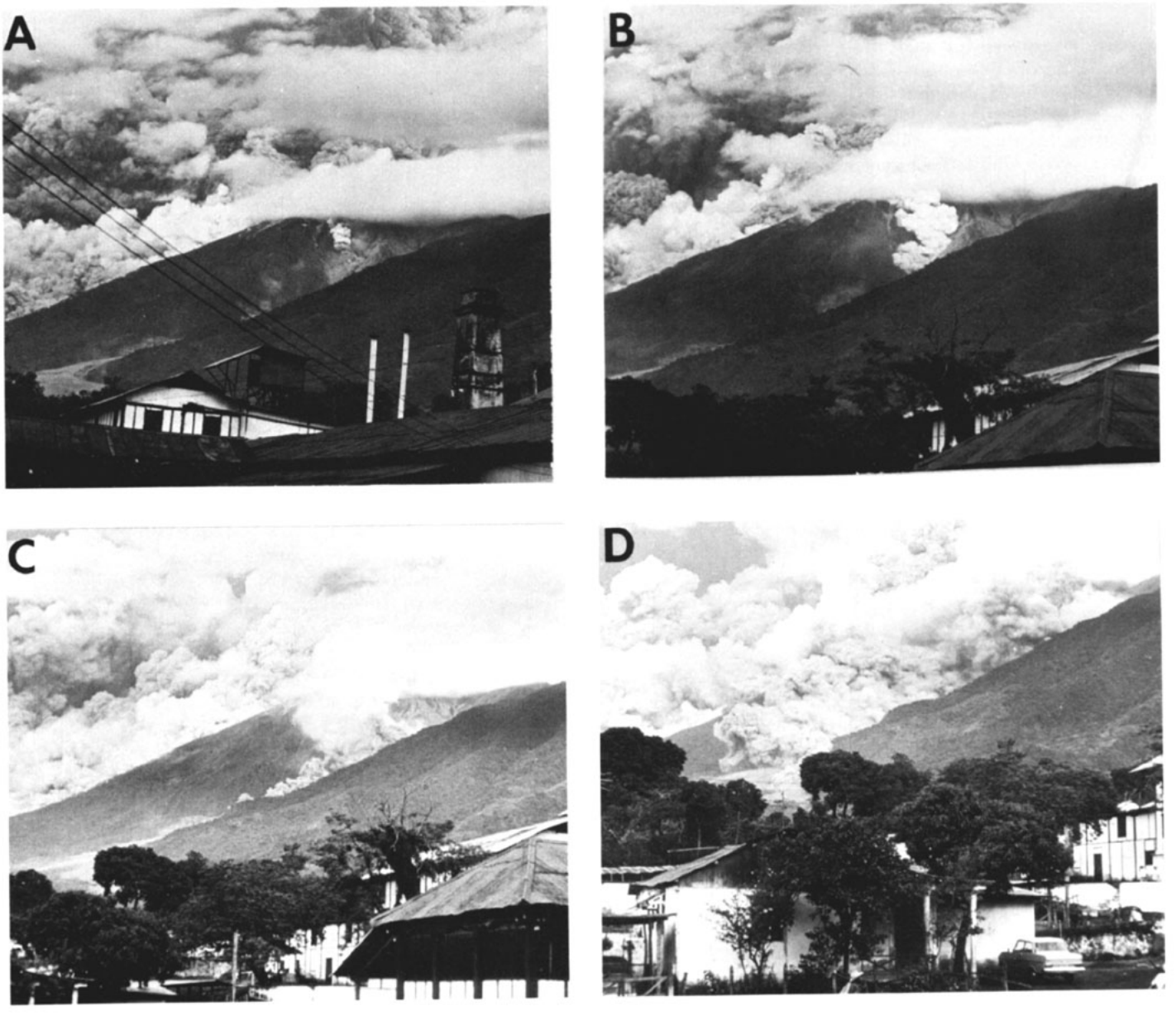

Figure 6. Time-lapse photographs of a single glowing avalanche. The vent of Fuego is 7.5 km from observation station. Vertical relief on Fuego is 2,300 m. A. Avalanche emerges from crater notch. Superjacent gas cloud is small and white. B. Avalanche just prior to reaching first major break in slope on the volcano flanks. C. Avalanche follows topographic low. Superjacent gas cloud changes color at break in slope, reflecting a change in the relative amounts of H_2O and dust. D. Avalanche emerging from valley, turns to east following the dominant topographic low. E. Avalanche sweeps past observation station.

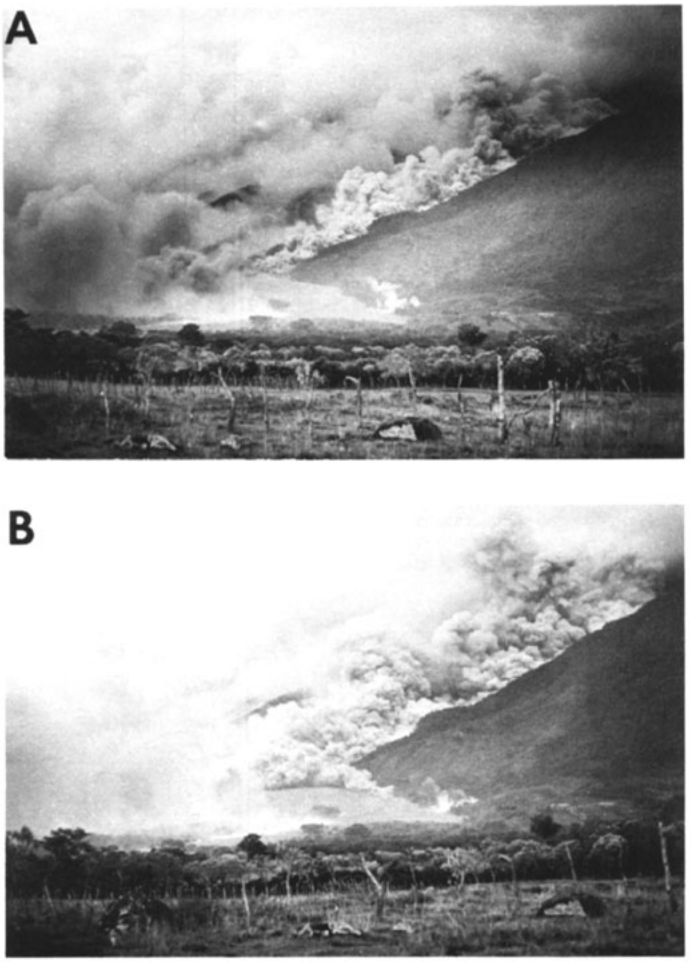

Figure 7. Time-lapse photographs of a second glowing avalanche that immediately followed the avalanche shown in Figure 6. A Superjacent gas cloud from previous avalanche is blown to the west by prevailing winds. Note the smoke from fires set in vegetation by preceding avalanches. Second glowing avalanche progresses down valley. B. Second glowing avalanche follows identical path to first glowing avalanche shown in Figure 6.

Figure 8. Aerial view of the intermittent stream valley known as Quebrada El Pajal (A). All light-colored deposits are the results of glowing avalanches from the 1974 eruption of Fuego (photo taken two months after eruption).

The weights of every grain in each size class were then summed to yield total weight for individual $\frac{1}{2}\phi$ intervals. From visual estimations, it was determined that the glowing avalanche deposit comprised 29% grains, 61% matrix, and 10% boulders (particles with A axes >30 cm). From this, weight frequency percentages could be calculated for each size interval.

Matrix. Each sample of matrix (two per sample site) was sieved at $\frac{1}{2}\phi$ intervals from -4.5ϕ to 4.75ϕ for 20 min in a Ro-Tap mechanical sieving device, and the appropriate weight-frequency percentages were calculated. Grain size statistics used are Folk's (1959) inclusive graphic statistics.

Shape Analyses

Sphericity. For each of the 26 grains sampled at each site, the long (A), intermediate (B), and short (C) axes were measured, and sphericity (that is, equidimensionality) was determined for each grain using the method of Krumbein (1941a). Zingg shapes (Zingg, 1935) were determined in conjunction with sphericity values. Grain sphericity data were divided into 25 to 32 mm, 33 to 64 mm, and 25 to 300 mm size ranges to check sphericity variations among different grain sizes.

Roundness. Roundness was determined for each of the 26 grains sampled at each site, using Krumbein's (1941a) method of assigning roundness by visually comparing grains with a series of images reproduced on paper. Grain roundness data were divided into 25 to 32 mm and 33 to 64 mm size ranges. Although Krumbein's chart at its original size is only directly comparable to particles in the 16 to 32 mm size range, the chart may confidently be used with grains up to 64 mm long-axis by holding the grain a short distance behind the chart when comparing for roundness. Particles larger than 64 mm were not used in roundness analysis, because Krumbein's chart could not be used for particles of this size.

OBSERVATIONAL EVIDENCE

Description

Each glowing avalanche from Fuego consisted of two parts: (1) the avalanche *per se,* or underflow, consisting of the main mass of hot fragments; and (2) a superjacent gas and dust cloud. At night, the incandescent nature of the avalanche was revealed by a series of white to red trails high on the volcano slopes. During the daytime,

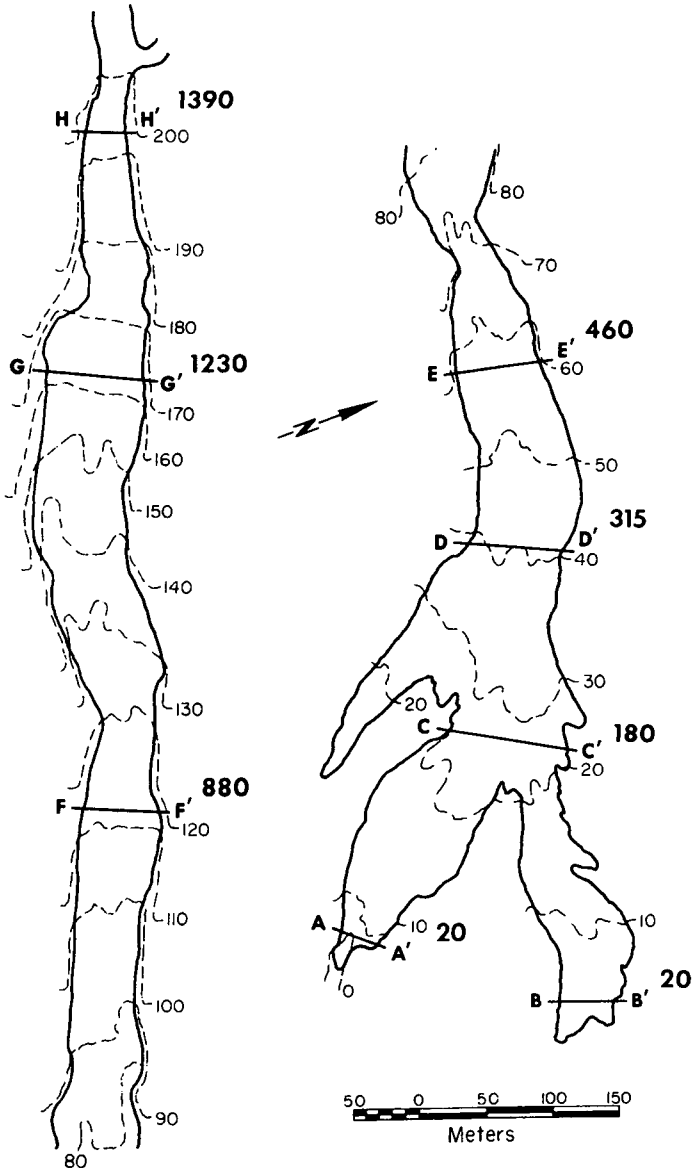

Figure 9. Map of glowing avalanche deposit at El Pajal. Note that the deposit is continuous and that the bottom of the left-hand portion attaches to the top of the right-hand portion of the diagram. Sampling traverse lines are numbered, each number indicating the distance in metres from the terminus of the deposit. Thus, line 315 is 315 m upflow from the terminus.

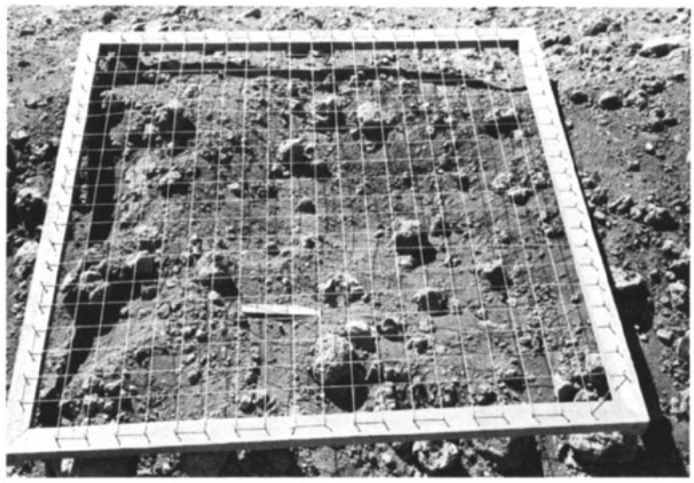

Figure 10. Random sampling grid used for selection of grains on the surface of the avalanche and in 1-m-deep pits.

Figure 11. Glowing avalanche deposit, with bark stripped off upflow side of trees to a height of 1.5 m above the postdepositional top of the avalanche (thickness of the avalanche deposit at this locality is 15 cm).

Figure 12. Grains of vesicular basalt, 20 cm in diameter lodged in the fork of a tree, 3 m above the postdepositional top of the avalanche.

the superjacent gas and dust clouds occluded the glowing particles in the underflow. Individual avalanches traveled some 7 km at an average speed of 60 km/hr.; they followed topographic lows. The time-lapse photographs (particularly Fig. 6B) suggest that a single flow may have moved in a succession of surges. After deposition, the debris from each avalanche was generally less than 2 m thick. Tree bark was scraped and battered to heights of at least 2 m above the surface of the deposits, while fragments of vesicular basalt up to 20 cm long were occasionally lodged in tree branches some 3 m above the ground surface (Figs. 11 and 12). A succession of glowing avalanches produced deposits up to 15 m thick in some of the ravines on Fuego's flanks.

Flow in the superjacent gas and dust clouds which accompanied each avalanche was turbulent (Fig. 6). The gas clouds were white when they emerged from the crater (Figs. 6A and B), but they be-

came light brown when they reached lower portions of the volcano flanks (Figs. 6C through 6E). Gas clouds increased in size with increasing distance from the crater and built to estimated heights of 1,000 m at distances as great as 6 km from the crater. After building vertically, the superjacent gas clouds were blown to the west-southwest by the prevailing wind (Fig. 7). No evidence was observed of a Peléan-type gas cloud flowing independently of the underlying avalanche as has been described for the devastating 1902 nuée ardente from Mount Pelé (Macdonald, 1972). At Fuego, superjacent gas clouds billowed above the same path as that followed by the underlying avalanche (Figs. 6 and 7).

Interpretation

The height of the gas and dust clouds associated with the glowing avalanches may be regarded as the result of the complex interaction of a number of variables, chiefly (1) amount of debris in the underflow, (2) temperature of the debris, (3) composition of the debris, (4) velocity of the avalanche, (5) velocity of ambient medium, (6) density contrast between ambient medium and the gas and dust cloud, (7) phreatic explosions, (8) phase changes, (9) chemical reactions, and (10) the amount of cold air entrapped in the moving debris.

The general increase in gas cloud height with increasing distance from the cone is considered to have been primarily the result of the gradual reduction in avalanche velocity with increasing distance of transport. Phreatic explosions are not considered to have been important on the southeastern flanks of the volcano, for most of the ravines and fans in this area were dry. Such explosions may have occurred on the southwest flanks where many of the ravines had running streams at the time of the eruption. However, the prevailing west-southwest wind prevented observations on this flank of the volcano.

Deposits of individual avalanches from this eruption cannot be distinguished in vertical section probably because the fine-grained dust of the gas and dust cloud was not deposited on top of each avalanche, or if it was, it was destroyed by subsequent avalanches. Had the dust entrained in the gas cloud been deposited on top of each underflow, then an excellent fine-grained marker would have been produced which would indicate the boundary between individual avalanches.

Determination of the role of gas in glowing avalanche flow has long been of interest. According to the earliest accounts (Anderson and Flett, 1903; Lacroix, 1903), the reduction of friction due to hot, expanding gas was recognized as the most important factor in giving a glowing avalanche both mobility and the ability to transport large blocks considerable distances (Macdonald, 1972). The origin of the friction-reducing gases has been subject to the most controversy. Early workers (Anderson and Flett, 1903; Fenner, 1923; Perret, 1937) proposed that each particle in a glowing avalanche is surrounded by an auto-initiated expanding gas envelope producing a buoyant, cushioning effect in the avalanche. Bemmelen (1949), working in Indonesia, suggested that the cushioning effect was due to expanding gases and "heated air." McTaggart (1960) proposed that mobility was provided by the violent expansion of cool, atmospheric air trapped during the transit of a glowing avalanche. Both "gas emission" and "entrapment of air" were reported in glowing avalanches produced by the 1968 eruption of Mayon Volcano (Moore and Melson, 1969).

Gas emission from fragments in the underflow is believed to have occurred during the downslope movement of the glowing avalanches from Fuego. Essential fragments from the avalanche deposits of 1974 contain irregular to spherical vesicles. Such vesicles indicate outgassing during flow (Murai, 1961). Additional evidence is the presence of breadcrust structures in some blocks observed on the avalanche after deposition. Breadcrust structure has been interpreted as an indication of gas production during flow (Moore and Melson, 1969).

Determination of the thickness of the main mass of moving debris (underflow) is important in understanding the flow mechanisms involved in glowing avalanche movement. Was the underflow gas-expanded? If so, how much expansion occurred? The scraping of bark from trees at least 2 m above the postdepositional surface of the underflow (Fig. 11) and the emplacement of basalt fragments in tree forks (Fig. 12) would suggest that during transportation the underflow may have been expanded to several times its postdepositional thickness.

However we would caution against the blind acceptance of such evidence. Inspection of Figure 11 will reveal that maximum stripping of tree bark has occurred on the upflow side, whereas the downflow side is virtually unaffected. Such an effect could be produced as a result of erosion by a gas-expanded underflow, or it could be the result of the conversion of kinetic to potential energy. The presence of the tree in the path of the moving underflow would cause fragments to be thrown vertically up the tree trunk on the upflow side — similar to the effect produced by a bridge abutment in a moving stream. The height to which upthrown particles would reach (h_{max}) may be calculated from the equation:

$$h_{max} = \frac{V^2}{2g}.$$

For the case shown in Figure 11, the location is near the terminus of the deposit, and thus the velocity was probably considerably lower than the average velocity of Fuego's glowing avalanches. Estimating v = 15 to 20 km/hr at this locality,

$$h_{max} = 0.89 \text{ to } 1.57 \text{ m.}$$

Thus the effects of erosion of the bark by upthrown particles may be expected to reach the heights shown in Figure 11, by the simple conversion of kinetic to potential energy.

Significant gas expansion of the underflow is not the only explanation possible for fragments lodged in tree forks (Fig. 12). They could bounce off larger fragments at the surface of the underflow, or be the products of moving waves of debris (surges) in a flow of irregular surface height. Whichever explanation is preferred, there can be little doubt that such evidence is equivocal. In the absence of direct observation, which is impossible, the nature of the flow in the underflow and the role of gas on underflow volume must be inferred from details of avalanche morphology, bedding, particle size, and shape. These data were obtained from the study of the avalanche deposits in Quebrada El Pajal (Figs. 5 and 8).

MORPHOLOGY

Description

Quebrada El Pajal is a small intermittent stream valley cut into the eastern flank of Fuego (Fig. 8). In October of 1974, glowing avalanches poured through a 60-m-deep notch in the eastern side of the crater rim, some of which funneled into Quebrada El Pajal at velocities timed at between 50 and 60 km per hour along the de-

scent path portrayed in Figure 13. Deposition of debris commenced 4 km from the vent where slope angle and avalanche velocity began to decrease.

Valley sides were devastated to maximum heights of some 10 m above the postdepositional surface of the underflow. The height of devastation was not the same on opposing sides of the valley. The locations of maximum devastation suggest that each avalanche followed a careening, sinuous path (Fig. 14). In devastated areas, the basal 5 m of the valley wall was littered with a veneer of basalt fragments and dust. In the uppermost 5 m of the valley walls, devastation was restricted to extensive damage of vegetation, such as stripping and charring of leaves, breaking of thin tree limbs, and the deposition of some dust.

Percussion marks (Fig. 15) were gouged into the north wall near the 80-m contour line (Fig. 14). Seven major percussion marks were measured between 1.5 m and 3 m above the present surface of the avalanche deposit. Six were subhorizontal linear grooves, which dipped downflow between 12° and 38°, most probably reflecting the impact of particles moving downflow roughly parallel to the wall. The largest measured 100 cm long by 20 cm high by 4 cm deep. One was an oval impact mark, measuring 20 × 15 × 6 cm, and was probably the result of a more direct impact.

When studied, the avalanche deposit had not received any rainfall, and the surface of all particles was whitened with dust, making the avalanche very distinctive from underlying black deposits which represent the products of the 1973 eruption of Fuego (Fig. 8). Minor quantities of charred wood fragments were present. Ash and lapilli lay on top of blocks. The surface was loose and unconsolidated, and settled and compacted underfoot as much as three months after deposition. This is in direct contrast to other canyons where the avalanche surface hardened almost immediately following deposition.

Avalanche deposits in El Pajal are confined between steep valley walls in uppermost portions of the valley (Figs. 8 and 14). Here the irregular avalanche surface is composed mainly of randomly distributed lapilli and ash with occasional blocks. At a lower altitude, the valley suddenly opens onto a broad fan. Thus distal portions of the glowing avalanche deposit are not confined by valley walls, but are spread out over this fan (Fig. 8), and exhibit depositional features resembling channels and levees (Fig. 16).

Channels, apparently determined by pre-avalanche topography,

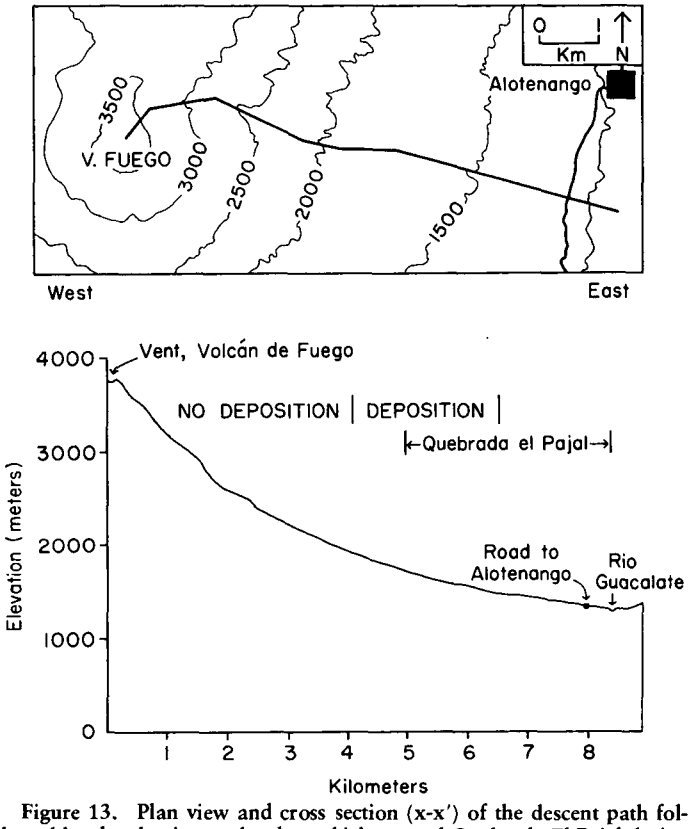

Figure 13. Plan view and cross section (x-x') of the descent path followed by the glowing avalanches which entered Quebrada El Pajal during the October 1974 eruption of Fuego. Note that deposition only occurred between 4 and 7 km from the vent.

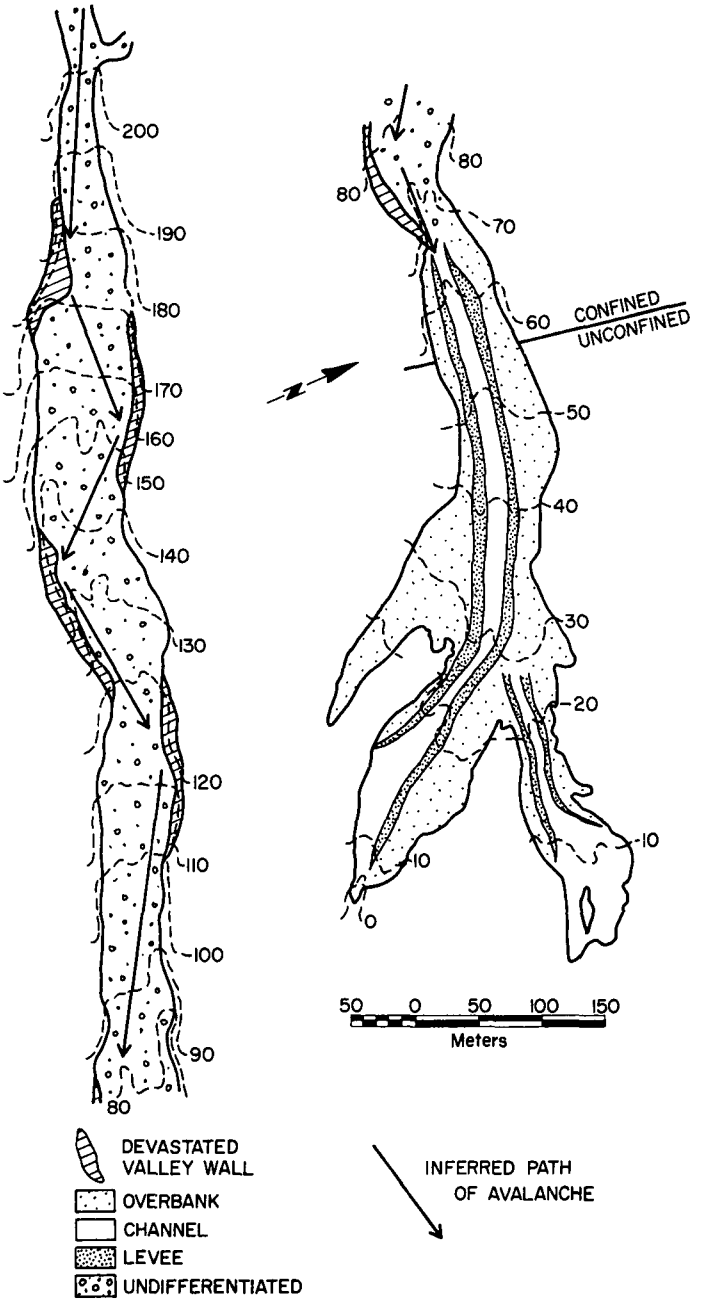

Figure 14. Contour map of glowing avalanche deposits in El Pajal showing the inferred path of travel of avalanches, areas of heaviest vegetative devastation on the valley sides, and depositional environments.

Figure 15. Percussion marks in the unconsolidated valley walls of El Pajal indicating lateral motion of particles.

Figure 16. Channel (C), levee (L), and overbank (O) environments on the surface of the unconfined portion of the avalanche deposits of El Pajal.

Figure 17. Channel environment of the glowing avalanche photographed nine months after deposition. Fines have been winnowed out by running water, and the concentration of blocks in the channel environment is readily apparent.

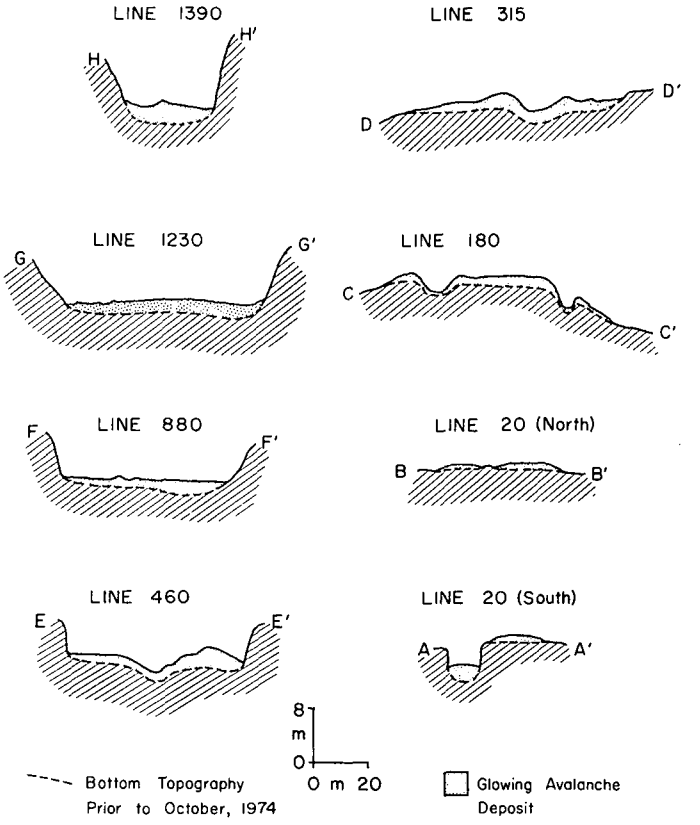

Figure 18. Cross sections of glowing avalanche deposits in El Pajal. Lines of cross section coincide with sample traverse lines (Figs. 9 and 14).

are filled with ash and blocks (Fig. 17) and generally lack lapilli-sized particles. Ridges marginal to the channels, here called leveees, bound both sides of a channel (see Fig. 18, lines 20 north, 180, and 315). Material in many levees consists largely of lapilli, and is better sorted than channel or overbank deposits. Where channels and leveees are present, all peripheral areas are termed overbank. Overbank deposits are less well sorted than are levee deposits. Several superimposed lobes were observed in disal portions of the avalanche deposit. The terminus of any single avalanche is steep and relatively coarse-grained (Fig. 19).

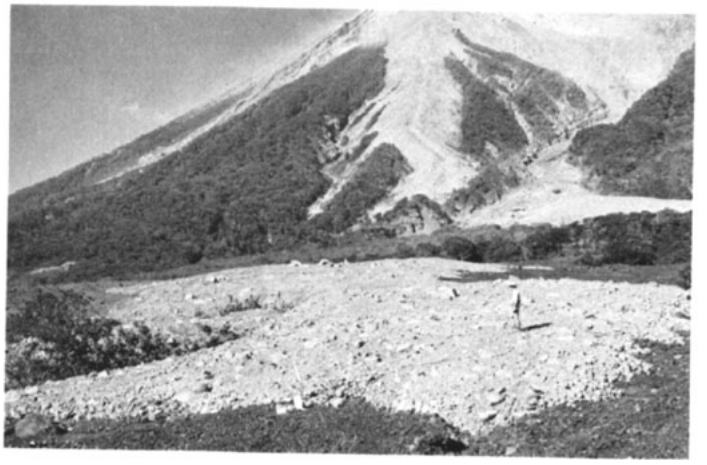

Figure 19. Dust-whitened northern terminal lobe of the glowing avalanche deposit at Quebrada El Pajal.

All blocks in the unconfined portion are restricted to the channels; the largest accumulation occurs between 290 m and 480 m upslope from the terminus of the deposit. One block is 5 m long (Fig. 20). Nearly all of the blocks are of andesitic composition.

Interpretation

The careening sinuous flow pattern indicated by the locations of areas of maximum devastation in the confined segment of the valley may have been inititated by the protuberance in the valley wall between the 170- and 180-m contours (Fig. 14). Such a flow pattern suggests that the conservation of momentum was high in each flow.

Devastation of foliage and tree limbs some 10 m above the avalanche surface was probably the result of hurricane winds associated with the turbulently flowing gas and dust clouds. The causes of percussion marks and the veneer of fragments up to 5 m above the avalanche surface are more problematical, and several interpretations are possible.

Such erosion and depositon may reflect the fact that the underflow was gas-expanded during transportation. (The presence of numerous fragments of ash and laipilli on the top of blocks in the avalanche may suggest that the avalanche deflated during or immediately after deposition). If gas expansion is the sole explanation for these erosional and depositional features on the valley wall, then gas expansion resulted in a volume increase of the underflow of between three and five times its postdepositional thickness.

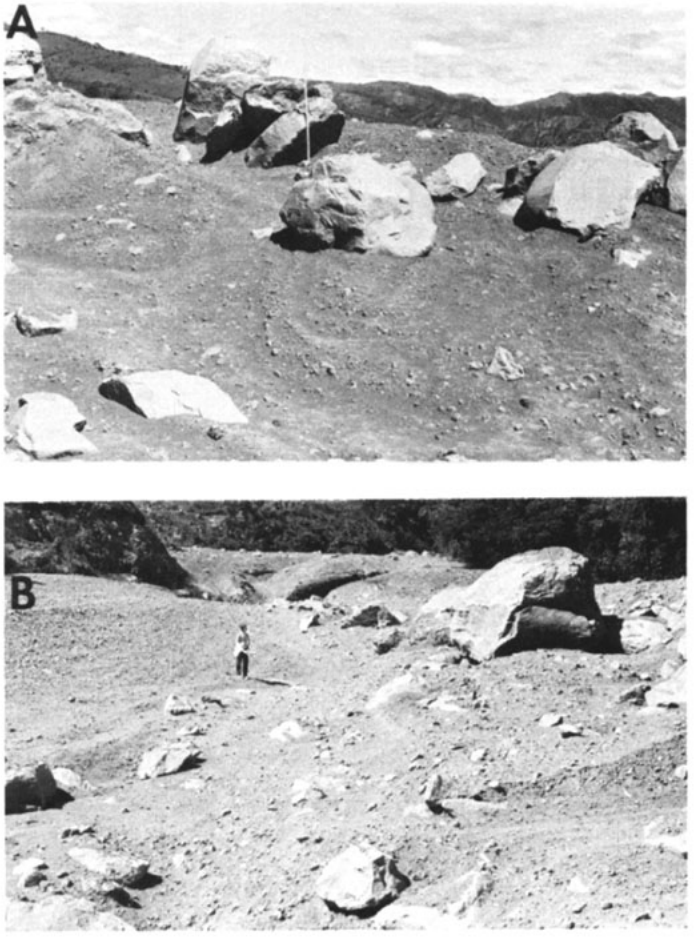

Figure 20. Boulders (blocks) in the El Pajal avalanche deposit. Large boulder in B is 5 m in diameter.

However, several other explanations are possible, which do not necessitate such a large increase in volume. The underflow may have been shorter and thicker during transportation. Reduction in slope and concomitant loss of velocity would result in a gradual deposition of material from the underflow, thus causing the underflow to elongate and thin in its final stages of flow.

Alternately, in longitudinal profile, the underflow may be envisaged as a large wave of solid material flowing steadily down valley with superimposed smaller waves on its surface. Such a morphology is characteristic in debris flows, where the smaller waves travel at higher velocities than the debris flow itself (Johnson, 1970, p. 435). The superimposed lobes noted in the distal portions of the glowing avalanche deposit at El Pajal may have originated as waves within a single flow, and which were preserved at the cessation of forward motion. Yet it would be difficult, if not impossible, for a 2-m-thick underflow to be comprised of smaller surface waves with the amplitude necessary to devastate valley walls to a height of 5 m without recourse to further superelevation of the surface of the underflow.

The underflow in El Pajal appears to have moved sinuously down valley. The outer edge of the underflow could be expected to be superelevated during sinuous flow. (In the same sense, the water surface of a meandering stream is superelevated near its outer bank.) The amount of outer bank superelevation ($\frac{1}{2}\ h_z$) is

$$\tfrac{1}{2}\ h_z = 2.3\frac{V^2}{g}\log_{10}\frac{R_2}{R_1}$$

where V is the mean velocity (60 km/hr), R_2 is the radius of curvature for the outer flow surface (210 m), R_1 is the radius of curvature of the inner flow surface (90 m), and g is the acceleration of gravity (Leliavsky, 1955, p. 124). For the confined segment of the valley, the amount of outer bank superelevation is

$$\tfrac{1}{2}h_z = 12\text{ m}.$$

This equation was derived from studies of moving water, and it may be expected that the high viscosity (relative to water) of the underflow would result in a reduction of the actual height of superelevation. Thus, the presence of fragments, dust, and percussion marks above the present avalanche surface may simply reflect the passage of surface waves in a superelevated underflow moving along a sinuous path.

The presence of well-defined levees and channels in distal portions of the avalanche (Fig. 14) indicates that the underflow acted as a non-Newtonian fluid with a high yield stress. These surface features are common on debris flows in which flowage is by a combination of laminar and plug flow (Johnson, 1970). The presence of levees and channels raises doubt as to the roles of gas and turbulent flow during transport of these glowing avalanches, for, if these avalanches were significantly expanded during transport (to 3 to 5 times their postdepositional volume), they would have great mobility, and flow would probably be turbulent.

An assessment of the mobility of glowing avalanches from the 1974 eruption of Fuego is possible using a plot of vertical height dropped (V_h) against the plot of horizontal distance of travel (H_d) (Fig. 21). This figure includes several different examples of mass transport processes, as well as glowing avalanches from the 1974 eruption of Fuego. As Francis and others (1974) and Sparks (1976) pointed out, the ratio V_h/H_d is a measure of mobility of these different processes. Francis and others (1974) noted that many glowing

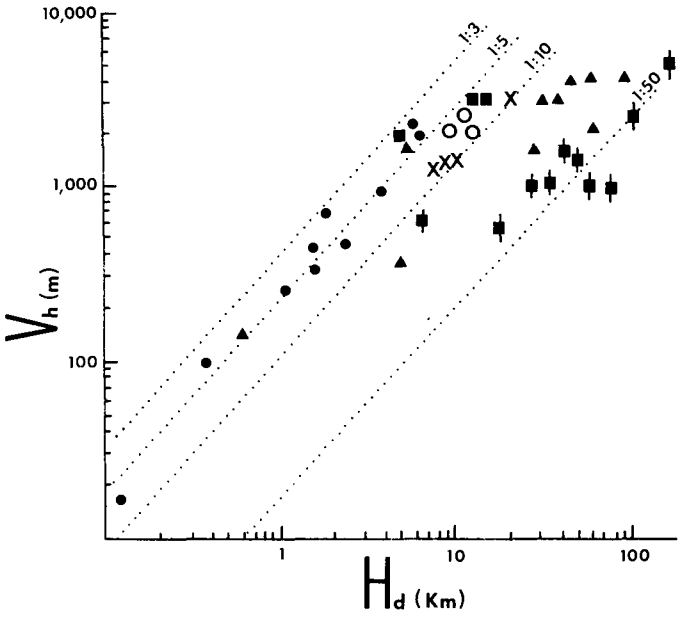

Figure 21. Relationship between the vertical height dropped (V_h) and the horizontal distance of travel (H_d) for glowing avalanches from Fuego, 1974, and other types of massive debris flow. Lines of equal V_h/H_d ratio are shown (data other than those for Fuego are from Sparks, 1976, Fig. 21, p. 183).

avalanches and pyroclastic flows are not significantly more mobile than landslides, despite their temperature. Data from the 1974 eruption of Fuego support this contention and throw some doubt on the role of gas as a lubricant in downslope flow of at least smaller glowing avalanches such as those produced by Fuego.

Variations in surface consolidation between El Pajal and other valleys reflect variations in the amount of fumerolic activity, which in turn is controlled by the original amount of water in the valleys. El Pajal was dry at the time of the eruption, and hence fumarolic activity was negligible, and the surface remained unconsolidated. Valleys of the southwest flanks had rivers flowing in them during the eruption and were characterized by a high degree of fumarolic acitivty, and the surface became case-hardened within a few days after deposition. Fumarolic acitivity was still continuing one year after deposition of avalanche material.

The andesite boulders are all considered to represent accidental fragments which were either torn from the vent during the eruption or were eroded from the walls of the canyons on the flanks of Fuego.

SIZE ANALYSES

Description

Thirteen grain size analyses of the glowing avalanche deposit reveal it to be extremely poorly sorted, strongly fine skewed, platykurtic, and with a mean grain size in the pebble (lapilli) range (Fig. 22). All grain size distributions are bimodal (Fig. 23), twelve have an intermodal low at -1.0ϕ, and one has an intermodal low at -0.5ϕ. There is no significant difference in grain size parameters between samples from the surface and samples taken from within 1-m-deep pits. There is no significant change in mean grain size along the length of the deposit. The greatest changes occur between environments in the unconfined portion of the flow.

Interpretation

Grain size distributions for El Pajal deposits closely resemble those classified as intermediate nuées ardentes by Murai (1961) (Fig. 24). Suggestion has been made that pyroclastic flow deposits will conform to Rosin's Law of crushing and will plot as a straight

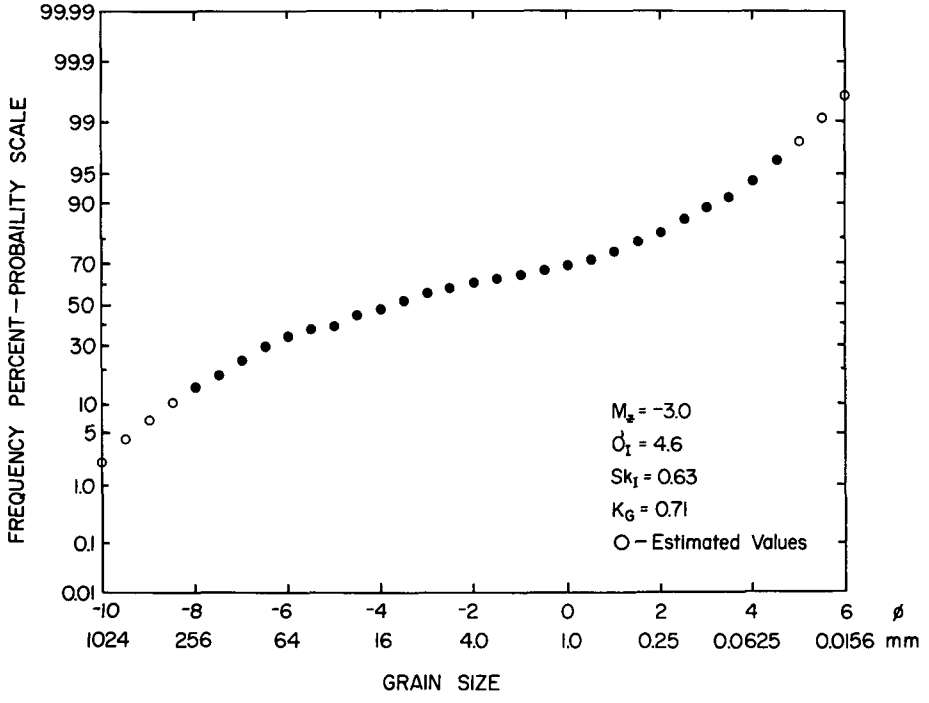

Figure 22. Average grain size distribution (log-probability plot) of avalanche deposits in El Pajal.

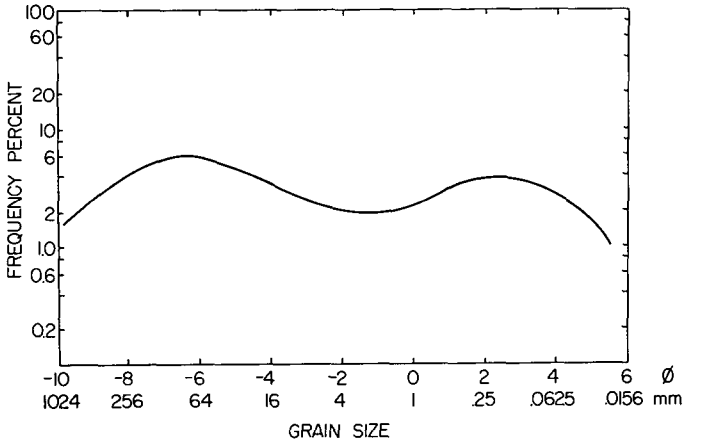

Figure 23. Average grain size distribution (semi-log plot) of avalanche deposits in El Pajal. (Data used for this plot are identical to those presented in Fig. 22.)

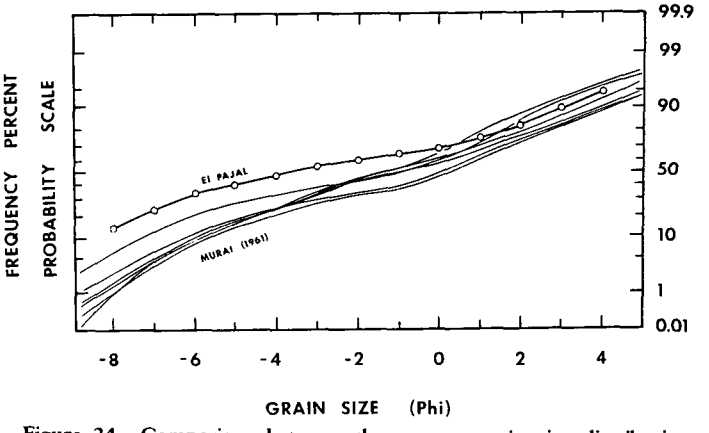

Figure 24. Comparison between the average grain size distribution curve for glowing avalanche deposits of El Pajal, and similar deposits in Japan classified as "intermediate nuées ardentes" by Murai (1961).

line on graph paper designed by Green and Yancy (1938) (Krumbein and Tisdel, 1940). However, Murai (1961) found that, in general, particle size distribution curves of pyroclastic flow deposits do not conform to Rosin's Law. Similarly, not one of the particle size distribution curves from El Pajal follows Rosin's Law.

The deficiency of material in the -1.0ϕ size interval is not peculiar to this particular deposit nor to pyroclastic flow deposits in general. Bimodal distributions occur in the size data of Moore (1934) and Murai (1961), with the majority exhibiting lows at -1.0ϕ (Table 1). The 0ϕ to -2ϕ interval has been recognized as being deficient in size distributions of sediments from many depositional environments (Pettijohn, 1957). Pettijohn studied approximately 1,000 published mechanical analyses and concluded that either material in the 0ϕ to -2ϕ (1 to 4 mm) size interval is never formed in nature in any appreciable volume or that this material is produced but is mechanically unstable and breaks down rapidly in transport.

Assuming that 0ϕ to -2ϕ particle sizes were produced in "sufficient" quantities in Fuego's vent, the only satisfactory explanation for the dearth is that particles in this size range disintegrated more rapidly than coarser and finer particles either in the vent and/or during transport. Particles of 0ϕ to -2ϕ size are dominant in numerous samples of airfall ash (Davies and others, 1978). Thus disintegration of particles of this size must have occurred dominantly during downslope movement of the glowing avalanche.

Increased sensitivity to abrasion of particles in the 0ϕ to -2ϕ size range may be related to texture, process, or to both. Pettijohn (1957) suggested that fragments in this size range are mechanically unstable because the grains of which they are composed are likely to make up a relatively large fraction of a single fragment, resulting in internal structural weakness between component grains. This inherent structural weakness would render the particles more mechanically unstable during transport than coarser and finer particles. The apparent long axis of the largest phenocryst in each of 100 particles of 0 to -2ϕ size fraction from El Pajal was measured. The average phenocryst length was 0.88 mm, or more than one-half of the average size of each individual particle in this size interval. If Pettijohn's (1957) reasoning was sound, then individual particles in the 0ϕ to -2ϕ size range in this deposit may indeed have been mechanically nondurable.

The inferred selective destruction of 0ϕ to -2ϕ sized particles suggests that breakdown of fragments does occur during transport in glowing avalanches. It also indicates that significant amounts of mechanical breakdown appear to be restricted to only the least durable particles.

The disintegration of particles in the 0ϕ to -2ϕ size range could produce the intermodal low, and also account for a large amount of fine material in the deposit. Thus some of the finest grained material in the glowing avalanche may well be produced during transport as a result of mechanical degradation of unstable particles in the 0ϕ to -2ϕ size range.

TABLE 1. OCCURRENCE OF INTERMODAL LOWS IN BIMODAL GRAIN SIZE DISTRIBUTIONS OF PYROCLASTIC FLOW DEPOSITS

Source	Sample	Lowest ϕ-interval between coarse and fine modes					
		0.0	−0.5	−1.0	−1.5	−2.0	−2.5
Murai (1961)	Ai-1	x					
	Nn-P			x			
	Km-o			x			
	Km-1929			x			
	KS			x			
	Kt			x			
	Hr-u			x			
	D			x			
	Nm-1					x	
	Am-S			x			
	Am-O			x			
	KF			x			
Moore (1934)	53a			x			
	54a			x			
Present study	1			x			
	1a			x			
	CP1			x			
	CP1a			x			
	LP1a			x			
	OP1			x			
	OPla			x			
	CP2			x			
	CP2a			x			
	LP2		x				
	LP2a			x			
	CP3			x			
	CP3a			x			

The similar size distribution of samples taken from the surface and those taken from pits suggests (1) that no vertical size grading existed within the upper 1 m of the deposit and (2) that no significant modification of surface deposits occurred prior to sampling. Subsequent rains caused small streams to downcut completely through the deposit, enabling inspection of the total thickness of avalanche deposits. No size grading occurred throughout the total thickness. The lack of size grading suggests that movements under fluid and gravitational forces were inhibited during flow, indicating a high concentration of particles in the underflow. The poorly sorted nature of the deposits is further evidence of the high degree of concentration of particles. The ability of these glowing avalanches to transport very large boulders up to 7 km from the crater may be a reflection of the high degree of particle concentration, and not a result of underflow expansion by gas. Similarly, large boulders are transported great distances in debris flows, the yield strength alone being sufficient to support them (Johnson, 1970).

GRAIN SPHERICITY

Description

Grains (particles with A axes between 30 and 2.5 cm) were examined for variations in sphericity and roundness. Sphericity determinations were restricted to basaltic grains which comprised more than 95 percent of all grains in the glowing avalanche deposit in El Pajal. Seventy-five percent of all basaltic grains were spherical (Table 2).

Average sphericity values for surface and pit sites along sampling lines are listed in Table 3 by size class. The largest variation in average sphericity between samples from surface sites and those from beneath the surface (pits) is 0.4; that is, the sphericities are nearly identical.

Figure 25 graphically portrays the downflow average sphericity values for individual sampling lines and suggests that sphericity did not change significantly in this distance of transport.

Interpretation

The similarity of grain sphericities from the surface and the interior of the deposit indicates that grains were not sorted by shape during deposition. Lack of downflow change in sphericity has been noted for a variety of other natural environments and in tumbling-barrel experiments (Dobkins and Folk, 1970; Krumbein, 1941b; Plumley, 1948).

The large percentage of spherical grains in the glowing avalanche deposit is considered to be a result of the cooling history of the grains. Liquids inherently tend to form objects of minimum surface area. In a similar manner, the magma in Fuego's vent probably formed spherical blebs in which the degree of equidimensionality was governed by viscosity, the amount of vesiculation, and the

TABLE 2. SHAPE CLASSIFICATION FOR 1,254 RANDOMLY SELECTED BASALT GRAINS FROM THE GLOWING AVALANCHE DEPOSIT IN EL PAJAL

Sampling line	Spherical (%)		Disc-shaped (%)		Rod-like (%)		Bladed (%)		Total no. grains	
	Surface	Pit	Surface	Pit	Surface	Pit	Surface	Pit	Surface	Pit
20	70		15		11		4		102	
180	76	68	10	18	13	13	1	1	306	92
315	79		15		4		2		146	
460	72	78	19	10	8	11	1	1	155	74
880	75	74	16	18	6	4	3	4	152	23
1,230	75		12		12		1		103	
1,390	77		15		7		1		101	
$\bar{X}$ =	75	73	14	15	9	11	2	1	1065	189
$\bar{X}$ =	75		14		9		2		1254	

TABLE 3. AVERAGE SPHERICITY VALUES OF BASALTIC GRAINS FROM THE GLOWING AVALANCHE DEPOSIT IN QUEBRADA EL PAJAL

Sampling line	Average grain sphericity											
	Surface						Pit					
	25–32 mm		33–64 mm		25–300 mm		25–32 mm		33–64 mm		25–300mm	
	n		n		n		n		n		n	
20	30	0.74	30	0.78	102	0.76						
180	96	0.78	145	0.78	306	0.78	31	0.78	41	0.74	92	0.76
315	30	0.78	50	0.80	146	0.79						
460	46	0.77	66	0.79	155	0.78	33	0.77	22	0.78	74	0.77
880	39	0.76	63	0.78	152	0.77	4	0.76	10	0.75	23	0.74
1230	25	0.79	42	0.77	103	0.77						
1390	29	0.80	57	0.77	101	0.78						
$\bar{X}_{20-315}$	156	0.77	225	0.78	554	0.77	31	0.78	41	0.74	92	0.76
$\bar{X}_{460-1390}$	139	0.78	228	0.78	511	0.77	37	0.77	33	0.75	97	0.76
$\bar{X}_{20-1390}$	295	0.77	453	0.78	1065	0.77	68	0.77	74	0.74	189	0.76

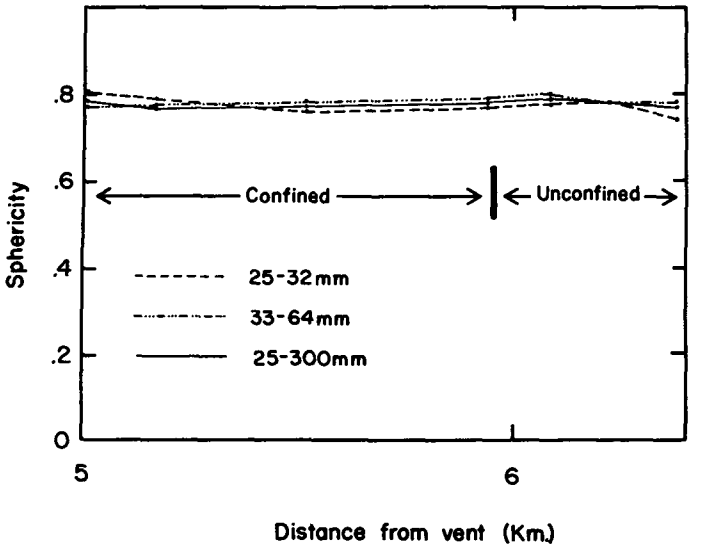

Figure 25. Plot of grain sphericities for basalt grains in glowing avalanche deposit of El Pajal (total number of grains = 1,254).

dynamic environment. At the cooling rate in Fuego's vent, viscosities may have been sufficiently high to prevent formation of perfect spheres. Vesiculation also would prevent formation of perfectly curved surfaces; nevertheless, it would still tend to form equidimensional blebs, assuming that expansion due to vesiculation proceeded at the same rate in all directions and that surface tension among all vesicles would keep the form intact. Thus the high percentage of spherical grains probably is a direct result of the magmatic origin of the grains and is not the result of transport or depositional processes.

TABLE 4. AVERAGE ROUNDNESS OF BASALT GRAINS FROM THE GLOWING AVALANCHE DEPOSIT IN EL PAJAL

Sampling line	Average grain roundness							
	Surface				Pit			
	25–32 mm	(A-axis)	33–64 mm	(A-axis)	25–32 mm	(A-axis)	33–64 mm	(A-axis)
	n		n		n		n	
20	30	0.33	30	0.34				
180	96	0.36	145	0.37	31	0.29	41	0.32
315	30	0.34	50	0.36				
460	46	0.22	66	0.31	32	0.27	22	0.30
880	39	0.29	55	0.31	4	0.25	10	0.31
1230	25	0.30	42	0.28				
1390	29	0.29	57	0.29				
$\bar{X}_{20-315}$	156	0.35	225	0.36	31	0.29	41	0.32
$\bar{X}_{460-1390}$	139	0.27	220	0.30	36	0.27	32	0.30
$\bar{X}_{20-315}$	381	0.36			72		0.31	
$\bar{X}_{460-1390}$	359	0.29			68		0.28	
$\bar{X}_{20-1390}$	740	0.33			140		0.30	
$\bar{X}_{20-315}$	453				0.35			
$\bar{X}_{460-1390}$	427				0.29			
$\bar{X}_{20-1390}$	880				0.32			

TABLE 5. HIERARCHICAL ANALYSIS OF THE VARIATION IN ROUNDNESS OF BASALT GRAINS IN THE GLOWING AVALANCHE DEPOSIT IN EL PAJAL

Level	Source of variation of roundness	Degrees of freedom	Chi-square	F
	25–32 mm (A-axis)			
1	Between confined and unconfined segments of avalanche	2	20.2	2.87* (L1/L2)
2	Between sampling lines	8	28.2	(L1/L2)
3	Between sample locations within a sampling line	12	46.6	0.91 (L2/L3)
	33–64 mm (A-axis)			
1	Between confined and unconfined segments of avalanche	2	42.2	10.30† (L1/L2)
2	Between sampling lines	8	16.4	0.90
3	Between sample locations within a sampling line	12	27.2	(L2/L3)

* Value significant at 0.10 level.
† Value significant at 0.01 level.

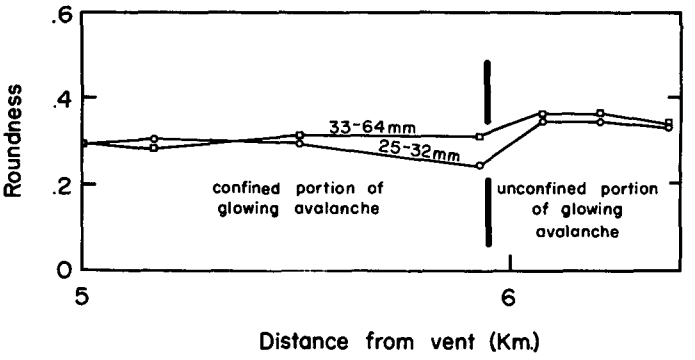

Figure 26. Plot of downflow variation in the roundness of basalt grains in the glowing avalanche deposit of El Pajal.

GRAIN ROUNDNESS

Description

Roundness determinations were also restricted to basalt grains. Average grain roundness was low; it ranged from 0.25 to 0.37 (Table 4). Equally low roundness values of 0.25 to 0.40 have been reported for pumice and scoria fragments from similar deposits in Japan (Murai, 1961). A small increase in grain roundness occurs in the distal, unconfined portion of the deposit in El Pajal from 0.29 to 0.35 (Table 4; Fig. 26). Williams (1957) similarly noted that pumice fragments are generally more rounded toward the distal ends of glowing avalanche deposits.

A hierarchical chi-square and associated "F" were undertaken to evaluate variation in grain roundness. Results for the 25 to 32-mm and 33 to 64-mm size classes are listed in Table 5, where $F_{L1}/_{L2}$ (25 to 32 mm) is significant at the 0.10 level and $F_{L1}/_{L2}$ (33 to 64 mm) is significant at the 0.01 level. This indicates that there is more variation in roundness betwen the confined and unconfined segments than between sampling lines.

Interpretation

The absence of significant downslope change in grain roundness in the confined segment of El Pajal may simply reflect the fact that the flow was dominantly laminar. Laminar flows, such as debris flows, have been demonstrated to be quite gentle. As Johnson (1970, p. 442) stated, "debris flows handle gently the objects they are transporting. Large boulders and fragile clasts such as fractured boulders and blocks of brittle shale . . . retain their respective identities during debris flow."

The small increase in grain roundness toward the terminus of the deposit is interpreted as the result of increased abrasion due to a higher frequency of grain-to-grain contact during flow in the unconfined portion. Grains at the snout of moving debris flows frequently roll and collide with one another, and some increase in roundness is to be expected in distal portions of glowing avalanche deposits.

ACKNOWLEDGMENTS

This study was made possible through the financial support of the National Science Foundation, Office of International programs, under Grant OIP-74-20040, and the División Geológica, Instituto Geográfico Nacional de Guatemala. Additional financial support was received from the American Explorers Club, the Department of Geology of the University of Missouri at Columbia, and the National Science Foundation, under Grant GA-26026. Dr. Oscar Salazar of the División Geológica, Instituto Geográfico Nacional de Guatemala, was responsible for the well-organized logistical support received during three field seasons. Bruce Hunter, Jake Dann, Dave Hyde, and Carl Nelson assisted in the field studies. Chiqui Bonis and Fraterno Vila Betoret provided generous hospitality in Guatemala. The administrators of Fincas Capetillo and San Diego kindly allowed free access to their properties.

Fruitful discussions concerning the 1974 eruption of Fuego were held with Russell F. Burmester, Dwight R. Crandell, Michael G. Foley, Glen Himmelberg, Bruce Hunter, Peter W. Lipman, Dan Miller, Donald R. Mullineaux, Kenneth Segerstrom, John M. Sharp, Jr., Richard E. Stoiber, and Ray E. Wilcox. The manuscript was reviewed by Dwight R. Crandall, Michael G. Foley, Bruce Hunter, Dan Miller, Kenneth Segerstrom, John M. Sharp, Jr., and Howel Williams.

The electron microprobe analyses were performed by C. K. Barsky and Glen Himmelberg on an instrument purchased by the University of Missouri with the assistance of the National Science Foundation, Grant GA-18445.

REFERENCES CITED

Anderson, T., and Flett, J. S., 1903, Report on the eruptions of the Soufrière in St. Vincent, 1902, and on a visit to Montagne Pelée, in Martinique: Royal Soc. London Philos. Trans. ser. A., v. 200, p. 353–553.

Bemmelen, R. W. van, 1949, The geology of Indonesia, *in* General geology of Indonesia and adjacent Archipelagoes (Vol. 1A): The Hague, U.S. Govt. Printing Office, 732 p.

Bonis, S. B., and Salazar, O., 1973, The 1971 and 1973 eruptions of Volcan deFuego, Guatemala, and some socio-economic considerations for the volcanologist: Bull. Volcanol. v. 37, p. 394–400.

Davies, D. K., Combs, M. J., and Bonis, S. B., 1978, Airfall tephra from the 1974 eruption of the volcano Fuego, Guatemala: Geol. Soc. America Bull., v. 89 (in press).

Dobkins, J. E., and Folk, R. L., 1970, Shape development on Tahiti-Nue: Jour. Sed. Petrology, v. 40, p. 1167–1203.

Fenner, C. N., 1923, The origin and mode of emplacement of the great tuff deposit of the Valley of Ten Thousand Smokes: Natl. Geog. Soc. Contr. Tech. Papers, Katmai Ser., No. 1, 74 p.

Folk, R. L., 1959, Petrology of sedimentary rocks: Austin, Texas, Hemphill's, 154 p.

Francis, P. W., Roobal, M. J., Walker, G.P.L., Cobbald, P. R., and Coward, M., 1974, The San Pedro and San Pablo volcanoes of northern Chile and their hot avalanche deposits: Geol. Rundschau, v. 63, p. 357–388.

Green, M. R., and Yancey, H. F., 1938, Expression and interpretation of the size composition of coal: Am. Inst. Mineralog. and Metallurg. Eng. Tech. Pub. 948.

Hay, R. L., 1959, Formation of the crystal-rich glowing avalanche deposits of St. Vincent, B.W.I.: Jour. Geology, v. 67, p. 540–562.

Johnson, A. M., 1970, Physical processes in geology: San Francisco, Freeman, Cooper, and Co., 571 p.

Krumbein, W. C., 1941a, Measurement and geological significance of shape and roundness of sedimentary particles: Jour. Sed. Petrology, v. 11, no. 2, p. 64–72.

——1941b, The effects of abrasion on the size, shape, and roundness of rock fragments: Jour. Geology, v. 49, p. 482–520.

Krumbein ,W. C., and Tisdel, F. W., 1940, Size distribution of source rocks of sediments: Am. Jour. Sci., v. 238, no. 4, p. 296–305.

Lacroix, A., 1903, L'eruption de la montagne Pelée en janvier, 1903: Acad. Sci. Comptes Rendus, v. 136, p. 442–445.

Leliavsky, S., 1954, An introduction to fluvial hydraulics: London, Constable and Co., 75 p.

Macdonald, G. A., 1972, Volcanoes: Englewood Cliffs, N.J., Prentice-Hall Inc., 510 p.

McTaggart, M. C., 1960, The mobility of nuées ardentes: Am. Jour. Sci., v. 258, p. 369–382.

Middleton, G. V., 1966-1967, Experiments on density and turbidity currents. Parts I–III: Canadian Jour. Earth Sci., v. 3, p. 523–546, 627–637; v. 4, p. 475–505.

Moore, B. N., 1934, Deposits of possible nuée ardente origin in the Crater Lake region, Oregon: Jour. Geology, v. 42, p. 358–375.
Moore, T. G., and Melson, W. G., 1969, Nuées ardentes of the 1968 eruption of Mayon Volcano, Phillipines: Bull. Volcanol. ser. 2, v. 33, p. 600–620.
Murai, I., 1961, a study of the textural characteristics of pyroclastic flow deposits in Japan: Earthquake Research Inst. Bull., v. 39, p. 133–248.
Perrett, F. A., 1937, The eruption of Mt. Pelée 1929–1932: Washington, D.C., Carnegie Inst. Washington, 126 p.
Pettijohn, F. J., 1957, Sedimentary rocks: New York, Harper and Brothers, 718 p.
Plumley, W. J., 1948, Black Hills, terrace gravels: A study in sediment transport: Jour. Geology, v. 56, p. 526–577.
Pough, F. H., and Mulford, J. W., 1957, The Cranbrook Central American volcano expedition: Cranbrook Inst. Sci. Newsletter, v. 27, p. 25–27.
Rose, W. I., 1973, Nuée ardente from Santiaguito volcano, April 1973: Bull. Volcanol., v. 37, p. 365–371.
Rose, W. I., Bonis, S. B., Stoiber, R. E., Keller, M., and Bickford, T., 1973, Studies of volcanic ash from two recent Central American eruptions: Bull. Volcanol., v. 37, p. 338–364.
Sapper, K., 1927, Volkankunde: Stuttgart, J. Engelhorns Nachf., 424 p.
Sheridan, M. F., and Updike, R. G., 1975, Sugarloaf Mountain Tephra — A Pleistocene deposit of base-surge origin in northern Arizona: Geol. Soc. America Bull., v. 86, p. 571–581.
Smith, R. L., 1960, Ash flows: Geol. Soc. America Bull., v. 71, p. 795–842.
Sparks, R.S.J., 1976, Grain size variations in ignimbrites and implications for the transport of pyroclastic flows: Sedimentology, v. 23, p. 147–188.
Stoiber, R. E., 1974, Volcanology: Nicaragua, El Salvador, Guatemala: Hanover, N.H., Dartmouth College, 125 p.
Taneda, S., 1954, Geologic and petrologic studies on the "Shirasu" in South Kyushu, Japan, part I, prelim. note: Kyushu Univ. Fac. Sci. Mem., ser. D., Geology, v. 4, no. 2, p. 167–177.
——1957, Geological and petrolgical studies of the "Shirasu" in South Kyushu, Japan, part II, prelim. note: Kyushu Univ. Fac. Sci. Mem., ser. D, Geology, v. 7, no. 2, p. 91–105.
Taneda, S., Mujachi, S., and Nishihara, M., 1957, Geologic and petrologic studies of the "Shirasu" in South Kyushu, Japan: Part III, The "Shirasu" in the Tsuruda-Hiwaki-Koriyama area, north of Kagoshima City: Kyushu Univ. Fac. Sci. Mem., ser. D., Geology, v. 6, no. 2, p. 107–127.
Williams, Howel, 1957, Glowing avalanche deposits of the Sudbury Basin: Ontario Dept. Mines 65th Ann. Rept., v. 65, p. 57–89.
——1960, Volcanic history of the Guatemalan Highalands: California Univ., Berkeley, Pubs. Geol. Sci., v. 38, p. 1–86.
Zingg, T., 1935, Beitrag zur Schotteranalyse: Schweizer Mineralog. u. Petrog. Mitt., v. 15, p. 39–140.

MANUSCRIPT RECEIVED BY THE SOCIETY JANUARY 29, 1976
REVISED MANUSCRIPT RECEIVED DECEMBER 16, 1976
MANUSCRIPT ACCEPTED FEBRUARY 8, 1977